# Transfer patterning of large-area graphene nanomesh via holographic lithography and plasma etching

Junjun Ding, Ke Du, Ishan Wathuthanthri, Chang-Hwan Choi, Frank T. Fisher, and Eui-Hyeok Yang[a)]
*Department of Mechanical Engineering, Stevens Institute of Technology, Castle Point of Hudson, Hoboken, New Jersey 07030*

(Received 4 August 2014; accepted 3 September 2014; published 11 September 2014)

The authors present a high-throughput fabrication technique to create a large-area graphene nanomesh (GNM). A patterned negative photoresist layer was used as an etch mask atop chemical vapor deposition grown graphene on Cu foil. Shielded by the periodic nanopatterned photoresist mask, the graphene layer was selectively etched using $O_2$ plasma, forming a GNM layer. A poly(methyl methacrylate) layer was spun on the GNM atop copper foil, and the GNM was subsequently transferred onto a $SiO_2$/Si substrate by etching away the copper foil. Large-area ($5 \times 5$ cm), periodic (500 and 935 nm in pitch), uniform, and flexible GNMs were successfully fabricated with precisely controlled pore sizes (200–900 nm) and neck widths (down to $\sim$20 nm) by adjusting the pattern generation of holographic lithography and the $O_2$ plasma etching process parameters. This holographic lithography-based transfer method provides a low-cost manufacturing alternative for large-area, nanoscale-patterned GNMs on an arbitrary substrate.
© *2014 American Vacuum Society*. [http://dx.doi.org/10.1116/1.4895667]

## I. INTRODUCTION

Graphene, a single atomic plane of graphite, has been widely studied because of its remarkable electronic properties, including extremely high mobility,[1,2] tunable carrier type, and density.[2,3] There have been numerous applications sought after in nanoelectronics,[4–6] chemical sensors and biosensors,[7–10] solar cells,[6,11,12] and batteries.[13–16] Graphene nanomeshes (GNMs) and graphene nanodots (GNDs) have been used for gas sensors,[9,17] light harvesting,[18,19] surface enhanced Raman spectroscopy,[8] and bioimaging.[20]

Several different process methods have been reported to fabricate GNMs.[21–30] Quasi-periodic hexagonal GNMs were created by the combination of nanoimprint lithography and block copolymer self-assembly, resulting in sub-10 nm neck widths.[22] GNMs with neck widths as small as 5 nm have been prepared by Duan's group using only block copolymer lithography.[23] GNMs have also been fabricated using anodic aluminum oxide (AAO) as an etch mask.[26] Another high-throughput fabrication method has been developed by utilizing self-assembled nanospheres as the mask for plasma etching of graphene at low power.[25] In an alternative approach, nanospheres have been used to prepare a porous metal film as the etch mask for manufacturing GNMs.[24] Rather than etching graphene to produce GNMs, nanosphere lithography has also been applied to create nanostructured substrates for CVD growth of GNMs with smooth edges.[27] The aforementioned lithography methods, however, result in mesh periods that are constrained by the feature size of the mask layers (block copolymer, AAO membranes, or nanospheres), which limits their design flexibility. Furthermore, such nanomaterials-based template methods are not effective in providing pattern regularity over a large area. Other micro/nano processing methods involving e-beam lithography[18] or two-photon polymerization[31,32] are either time consuming or not cost-effective. On the other hand, holographic lithography provides a flexible way to quickly generate large area (full wafer scale) periodic nanopatterns with tunable pattern periodicity.[33–37]

Here, we demonstrate a new high-throughput fabrication process to create large-area GNMs through the combined use of holographic lithography, $O_2$ plasma etching, and layer transfer techniques, in which the pattern sizes and periods are easily controlled by adjusting process parameters. We directly pattern GNMs on copper, and then transfer the patterned graphene layer onto an arbitrary substrate. The key element of the process is to use a trilayer polymer stack consisting of negative photoresist, antireflective coating (ARC), and positive photoresist for the pattern transfer. By incorporating a sacrificial layer of positive photoresist between the ARC and graphene, we lift the multilayered polymer off the patterned graphene. Exposed by the nanopatterned negative photoresist, the unprotected areas of ARC, positive photoresist, and graphene layers are etched away using a single $O_2$ plasma etching step. We show that this method enables the fabrication of large-area, periodic, uniform GNMs with precisely tuned periodicity and neck width. Finally, we characterize the periodicity, uniformity, and the spatial resolution of the fabricated GNMs using scanning electron microscope (SEM) and Raman spectroscopy.

## II. FABRICATION SCHEMES

Figure 1 shows the fabrication sequence of the GNMs. First, polymer layers consisting of positive photoresist, ARC, and negative photoresist are sequentially spun atop CVD grown graphene on copper foil [Figs. 1(a) and 1(b)]. Underneath the negative photoresist layer, the ARC is employed to minimize the standing wave effect on the sidewalls of the nanopores[35] that would be created in the

[a)]Electronic mail: eyang@stevens.edu



Redistribution subject to AVS license or copyright; see http://scitation.aip.org/termsconditions. Download to IP: 74.102.104.224 On: Thu, 11 Sep 2014 13:24:11

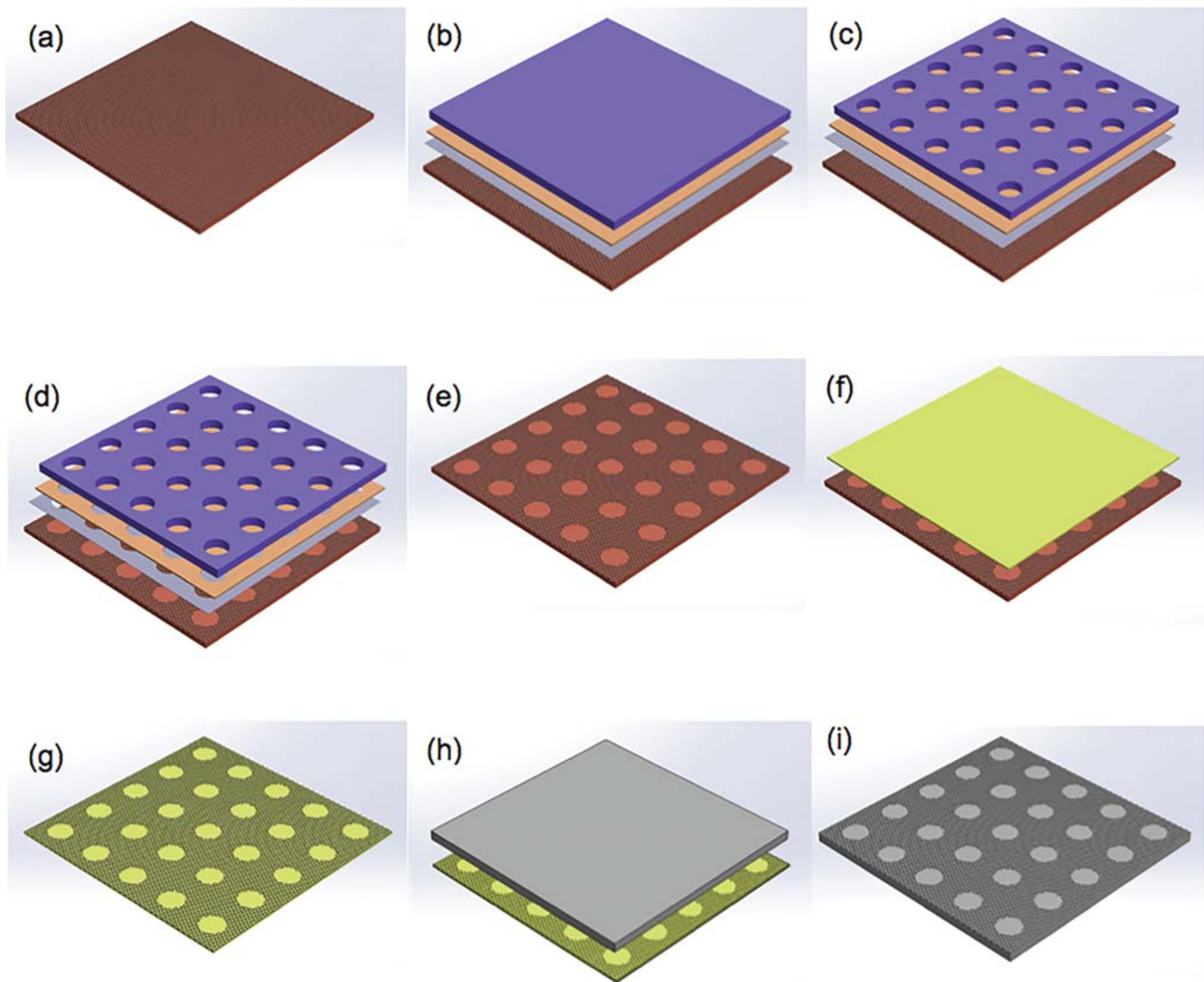


FIG. 1. (Color online) Schematic of nanofabrication processes of GNM for an arbitrary substrate. (a) The CVD graphene with a substrate of copper. (b) The graphene film is spin-coated with positive photoresist, ARC, and negative photoresist from bottom to top. (c) The negative photoresist is patterned using laser holographic lithography. (d) The stack is etched by $O_2$ plasma using the negative photoresist pattern as an etching mask. The ARC, positive photoresist, and graphene are all etched through in a single $O_2$ plasma etching step. (e) The positive photoresist, ARC, and negative photoresist are removed by a sonicated acetone bath, where the positive photoresist acts as sacrificial layer. (f) The GNM on copper is spin-coated with liquid PMMA as a supportive layer to transfer GNM. (g) The copper substrate is wet etched away by a copper etchant. (h) The GNM with PMMA support is contacted on an arbitrary substrate (Si substrate in this study) for the pattern transfer of the GNM. (i) The GNM is transferred to the substrate after removing the PMMA with acetone.

negative photoresist. Between the ARC and graphene layer, a layer of positive photoresist is used as a sacrificial layer[38] to enable lift-off of the multilayer polymer after the graphene has been patterned. A periodic pattern of nanopores is created on the top negative photoresist using holographic lithography[33] [Fig. 1(c)]. This nanopatterned negative photoresist opens up unprotected areas of ARC and positive photoresist layers that are etched away using $O_2$ plasma. After the ARC and positive photoresist have been etched through, the graphene layer is etched for approximately five additional seconds. Therefore, the ARC, positive photoresist, and graphene layers are etched by a single $O_2$ plasma etching step [Fig. 1(d)]. The polymer layers on top of the GNM are then removed using a sonicated acetone bath [Fig. 1(e)]. Next, a poly(methyl methacrylate) (PMMA) layer is spun atop the GNM on copper foil [Fig. 1(f)] to support the graphene patterns when the copper foil is etched away [Fig. 1(g)]. The GNM with the PMMA support is then transferred to a substrate with an arbitrary curvature [Fig. 1(h)], followed by adding approximately a microliter drop of liquid PMMA on the PMMA/GNM sheet to ensure full contact between the GNM and substrate. Finally, after the PMMA is removed by acetone the GNM on the arbitrary substrate remains [Fig. 1(i)].

## III. EXPERIMENTAL DETAILS

To fabricate the large-area nanopatterned mask for etching, CVD-grown graphene on copper foil ($5 \times 5$ cm) with a monolayer percentage greater than 95% from Bluestone Global Tech (Gratom-M1-Cu-02) was spin-coated with diluted positive photoresist (PR1–550A, Futurrex, Inc.) at



Redistribution subject to AVS license or copyright; see http://scitation.aip.org/termsconditions. Download to IP: 74.102.104.224 On: Thu, 11 Sep 2014 13:24:11

2000 rpm for 40 s and then annealed at 120 °C for 6 min, resulting in a 10 nm thick film. The positive photoresist was much easier to be removed by using solvent than the ARC or negative photoresist without damaging graphene and copper foil. A layer of ARC (XHRiC 16, Brewer Science) was spin-coated on top of the positive photoresist at 4000 rpm for 10 s and then baked at 175 °C for 1 min. The thickness of ARC was controlled to be 150 nm in order to cancel the standing waves on the sidewalls of the nanopores created in the negative photoresist by absorption of the reflective light. The negative photoresist (NR7–1500, Futurrex, Inc.) was spin-coated on top of the ARC at 3000 rpm for 40 s and then placed on a hot plate for 1 min at 150 °C. The thickness of this negative photoresist was controlled to be 800 nm in order to ensure that it had better mechanical durability and was thick enough to endure the $O_2$ plasma etching. The topmost negative photoresist layer was exposed twice by rotating the sample 90° at the surface plane using a two degrees of freedom Lloyd-mirror Interferometer with a UV laser (HeCd laser with the wavelength of 325 nm)[33] to generate a periodic nanopore pattern that covers the surface. In this experiment, the period was controlled to be either 935 or 500 nm by adjusting the exposure angle between the sample surface and the laser beam to be either 80° or 70°, respectively. At the 80° stage position, the sample was exposed at a dose of 3 mJ/cm$^2$ and then turned 90° to be exposed with an additional dose of 3 mJ/cm$^2$ for a total of 6 mJ/cm$^2$. The sample at the 70° stage position was exposed with dose of 6 mJ/cm$^2$ and then turned 90° to be exposed with another dose of 6 mJ/cm$^2$ for a total of 12 mJ/cm$^2$. Different exposure doses were used at different angles (for different pattern periodicity) to ensure contrast of the photoresist nanopatterns after development.

After the holographic pattern exposure, the sample was postexposure baked at 100 °C for 1 min and then developed in a negative photoresist developer (RD6, Futurrex, Inc.) for 12 s. The sample was cleaned with deionized water for 2 min and then blown dry by nitrogen gas. The underexposed area was removed by the developer, resulting in a nanopore pattern on the negative photoresist. The ARC and positive photoresist layers beneath the nanopore patterned negative photoresist were etched by $O_2$ plasma in the reactive-ion etching (RIE) mode (Phantom III, Trion Technology) with 50 W of power and an $O_2$ gas flow rate of 30 SCCM. The etch rate of the ARC and positive photoresist layers in the RIE process was ~4 nm/s, and it took 220 s to completely etch off the ARC and positive photoresist layers. Because the etch selectivity between ARC/positive photoresist (4 nm/s) and negative photoresist (1.5 nm/s) was high, the thick negative photoresist nanostructures still remain on top, preserving the nanopattern. Once the ARC and positive photoresist layers were etched through, the $O_2$ plasma then came into contact with the exposed graphene layer, which was etched through within only 5 s.

To remove the trilayer polymer atop the graphene nanopatterned layer, the sample was sonicated in an acetone bath for 3 h. As a sacrificial layer, the positive photoresist was dissolved in the acetone bath, stripping away the layers of the ARC and negative photoresist along with it. The sample was then rinsed with isopropanol alcohol, rinsed with deionized water, and blown dry with nitrogen. The large-scale (5 × 5 cm) flexible graphene nanopattern on copper foil substrate was thus obtained.

In order to retain the graphene nanopattern when transferring it onto a new substrate (i.e., $SiO_2$, Si), the sample was spin-coated at 4000 rpm for 40 s with a 495 000 molecular weight PMMA (Sigma-Aldrich) dissolved in anisole. The PMMA was then cured at 180 °C for 1 min, and the resulting PMMA thickness was approximately 60 nm. The copper foil was etched for approximately 12 h and then an additional 24 h in a fresh citric acid etchant (Transene) bath to ensure the complete removal of copper. Next, the PMMA/graphene stack was placed in a deionized water bath for 12 h to clean the citric acid before being transferred to a 90 nm $SiO_2$/Si substrate. Additional liquid PMMA solution was dropped on the cured PMMA layer to partially or fully dissolve the precoated PMMA on graphene. This step was introduced to enhance the contact between graphene and the target substrate by reducing any voids between the graphene and the substrate surface.[15] The new PMMA was slowly cured at room temperature for ~30 min. The sample was placed in an acetone bath at room temperature for 12 h, followed by another fresh acetone bath for an additional 12 h at room temperature to ensure complete PMMA removal. The transferred graphene nanopatterned sample was then cleaned with isopropanol alcohol and blown dry with nitrogen.

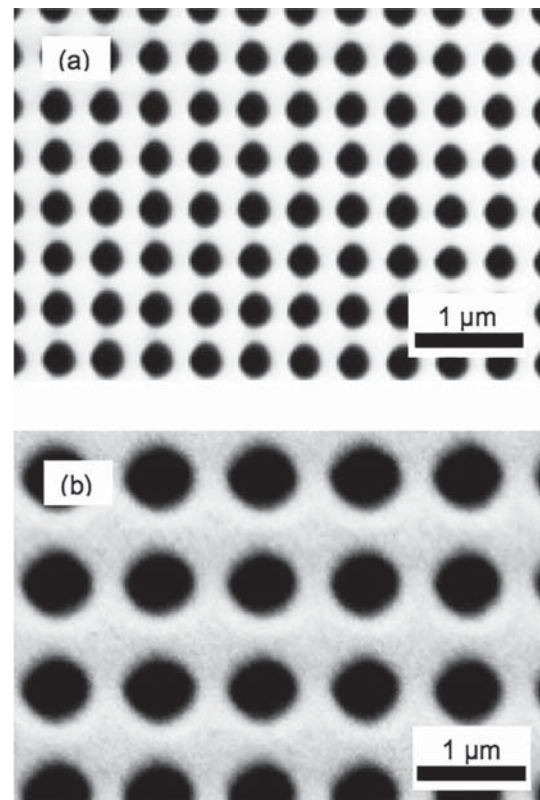


FIG. 2. SEM images (top views) of periodic nanopore patterns created on negative photoresist layer using laser holographic lithography. (a) Nanopore pattern with pitch of 500 nm. (b) Nanopore pattern with pitch of 935 nm.



Redistribution subject to AVS license or copyright; see http://scitation.aip.org/termsconditions. Download to IP: 74.102.104.224 On: Thu, 11 Sep 2014 13:24:11

## IV. RESULTS AND DISCUSSION

Figures 2(a) and 2(b) show the fabricated nanostructures on a negative photoresist prepared by laser holographic lithography with periodicities of 500 and 935 nm, respectively. The negative photoresist layer acts as a mask for the $O_2$ plasma to etch through the ARC, the positive photoresist, and the graphene. Therefore, the negative photoresist pattern determines the pattern on the graphene. A two-beam interference double exposure technique was used to generate a two-dimensional square array of nanopore patterns.[33] The pore size was regulated in the holographic lithography process by changing the exposure parameters.[35]

Figures 3(a) and 3(b) show cross-sectional views of the multilayered stack of the polymers after $O_2$ plasma etching. In order to reveal the cross-sectional view, the multilayered stack of negative photoresist, ARC, and positive photoresist atop graphene was milled by focused ion beam (FIB) *in situ* in the chamber of the SEM. The cross-sectional view shows the smooth vertical sidewall profile of the nanopore patterns of the negative photoresist layer, which was made possible by using the ARC interlayer.[35,38–43] During exposure, the incident light hitting the substrate interferes with the light reflected from the substrate. Without ARC, the intensities of reflective and incident light become comparable; this results in a significant standing wave in the vertical direction with a period equal to half of the laser's wavelength.[35] Adapted as a technique to eliminate this standing wave effect on the nanopores' sidewalls, the ARC underneath the negative photoresist was created with an optimal thickness of 150 nm.

Figures 4(a) and 4(b) show the GNMs left on a copper substrate with periodicities of 500 and 935 nm, respectively, after the sacrificial layer of a positive photoresist layer was removed with acetone. The negative photoresist and ARC polymers should be removed by using a strong acid, such as Piranha solution ($H_2SO_4 + H_2O_2$). However such a strong acid will corrode graphene and copper. Thus, the positive photoresist layer, which can effectively be removed by mild solution such as acetone, was used as a sacrificial layer to lift off the bilayer of the negative photoresist and ARC stack from the copper foil with GNMs. Due to the low imaging contrast between graphene and copper substrate, the SEM images noise was pronounced. However, the result still shows that the acetone was effective to remove the positive photoresist and lift off the bilayer of the negative photoresist and ARC stack without damaging the graphene and copper foil.

Figures 5(a) and 5(b) show SEM images of the large-area (5 × 5 cm) GNMs deposited on a $SiO_2$/Si substrate, with the pitch of 500 and 935 nm, respectively, after transfer from the copper substrate. The low-magnification SEM images show the ability to generate large area, periodic, and uniform nanopatterns of graphene. Based on the SEM images, the pore patterns were identified by using a Blob detection

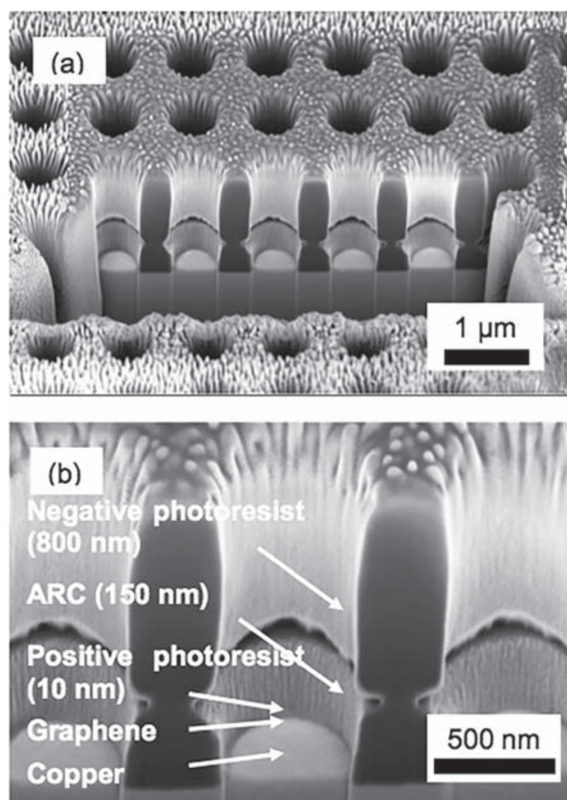


Fig. 3. Cross-sectional SEM images of the multilayered polymer stack after $O_2$ plasma etching. The cross section was made *in situ* in the SEM chamber by using FIB. The graphene layer between the positive photoresist and copper is not visible in this image due to its atomically thin nature.

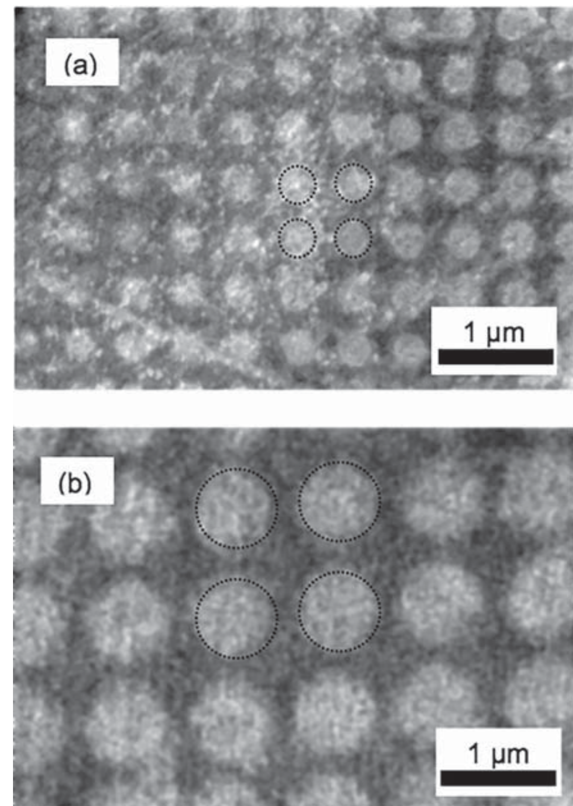


Fig. 4. (a) GNM patterned on a copper substrate with pitch of 500 nm, after the $O_2$ plasma etching through trilayer polymer stack and then the removal of the polymer stack by lift-off. (b) The GNM patterned on a copper substrate with pitch of 935 nm. The dashed line marked in each image is to clearly indicate the GNM patterns.



Redistribution subject to AVS license or copyright; see http://scitation.aip.org/termsconditions. Download to IP: 74.102.104.224 On: Thu, 11 Sep 2014 13:24:11

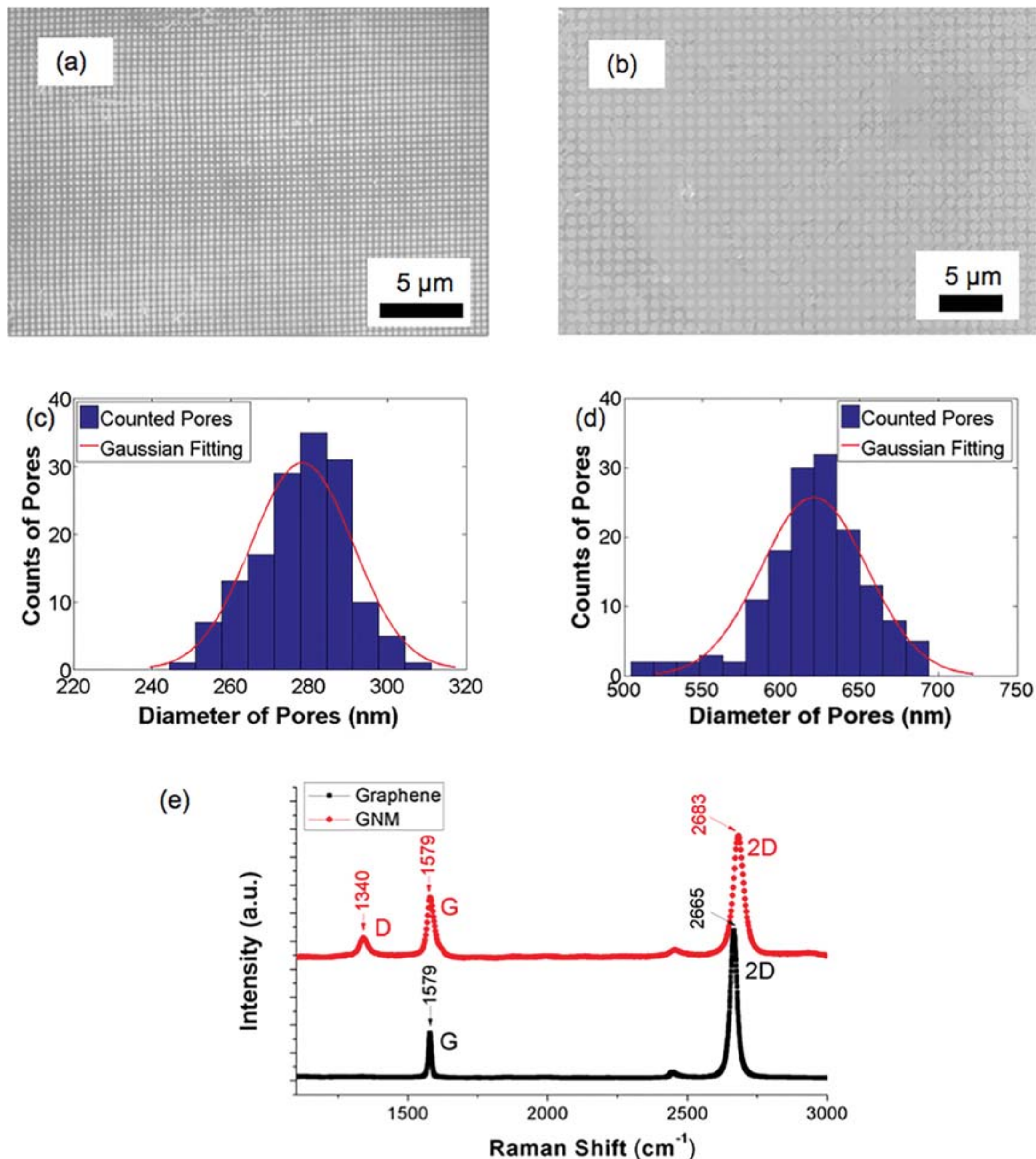


Fig. 5. (Color online) (a) and (b) SEM images of the GNMs (500 and 935 nm in pitch, respectively) transferred on $SiO_2$/Si substrate of a large-area (5 × 5 cm). (c) and (d) Histogram and Gaussian fit of the diameter of pores of the GNMs with the pitch of 500 and 935 nm, respectively. (e) Raman spectra of unpatterned graphene (lower line) and GNM (upper line) with a periodicity of either 500 or 935 nm.

method,[44] and the diameters of pores were calculated. As seen in the histogram and Gaussian fit of GNM pore diameters [Figs. 5(c) and 5(d)], the GNMs exhibit great uniformity with pore diameter of 354 and 533 nm with standard deviation of 23 and 33 nm for periodicity of 500 and 935 nm, respectively. The Raman spectra of the GNMs are shown in Fig. 5(e). The Raman spectra were obtained using a 14 mW, 632 nm laser with a spot size of 3 $\mu$m. The Raman spectra for both unpatterned graphene and GNMs were taken multiple times on different spots. The Raman spectrum of the unpatterned graphene [Fig. 5(e) (lower line)] shows G peak at 1579 cm$^{-1}$ and 2D peak at 2665 cm$^{-1}$; the GNMs [Fig. 5(e) (upper line)] shows D peak at 1340 cm$^{-1}$, G peak at 1579 cm$^{-1}$, and 2D peak at 2683 cm$^{-1}$. The 2D peak shifts from 2665 cm$^{-1}$ for unpatterned graphene to 2683 cm$^{-1}$ for patterned graphene, indicating the increased hole doping attributed to the nanopatterned edges in the GNMs, which absorb $H_2O$ or $O_2$ molecules.[8,18,45] Comparing‘ the Raman spectrum of the pristine graphene and the GNMs, the GNMs exhibit a D peak, which indicates the defects introduced by the nanopore patterning process. The Raman $I_D/I_G$ ratio (where $I_D$ and $I_G$ are the D-band and G-band Raman intensities), widely used to evaluate the graphene quality,[46] is related to the density of defects in the nanomesh and its edge roughness.[47] Here the Raman $I_D/I_G$ ratio is calculated to be 0.38–0.57 for the GNM samples, which is lower than most



Redistribution subject to AVS license or copyright; see http://scitation.aip.org/termsconditions. Download to IP: 74.102.104.224 On: Thu, 11 Sep 2014 13:24:11

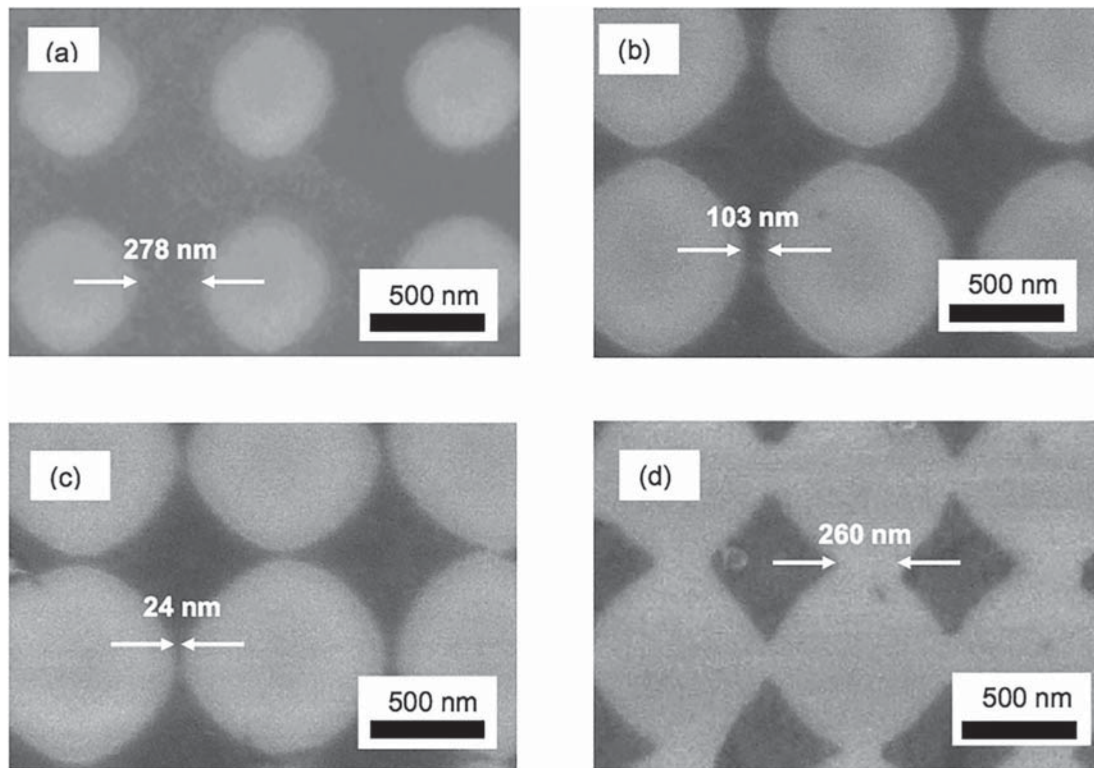


FIG. 6. Neck width control of GNMs with periodicity of 935 nm. (a) The GNM on a $SiO_2$ substrate with neck width of 278 nm. (b) The GNM on a $SiO_2$ substrate with neck width of 103 nm. (c) The GNM on a $SiO_2$ substrate with neck width of 24 nm. (d) The GNDs on a $SiO_2$ substrate with gap of 262 nm.

reported values of GNM, graphene nanoribbons, GND, and other graphene nanostructures etched from exfoliated graphene.[25,28,48,49] Notably, it is also lower than the smooth edged GNM directly grown on patterned Cu substrate.[27] The low $I_D/I_G$ ratio indicates a high GNM quality and smooth edges of pores created by the holographic lithography technique.

By controlling the etching parameters, the pore size of the GNM can further be adjusted precisely, as shown in Fig. 6. When the graphene layer is over-etched (e.g., more than 5 s) by $O_2$ plasma, the pore size of the GNM can be widened due to the slow but gradual lateral etching by $O_2$ plasma. Such a lateral etching effect due to the imperfect anisotropic etching characteristics of the $O_2$ plasma RIE process was employed to enlarge the pore size of the GNM. Figure 6 shows the resulting GNMs with periodicity of 935 nm by gradually increasing $O_2$ plasma etching time. As shown in Fig. 6(c), by controlling the total etching time in the $O_2$ plasma RIE process, the GNM neck width between two adjacent pores could be decreased to as small as 24 nm. With a further increase in etching time, the adjacent pores expanded to eliminate the neck, resulting in GNDs with gap distance of 260 nm [Fig. 6(d)].

## V. SUMMARY AND CONCLUSIONS

We have demonstrated a simple and effective method for fabricating large-area GNMs, utilizing holographic lithography followed by $O_2$ plasma etching of trilayer polymer stack consisting of negative photoresist, ARC, and positive photoresist. The Raman spectra have confirmed the structural integrity of GNMs with smooth edges. We have also shown that the pattern periodicity, pore size, and neck width are easily controlled by adjusting the processing parameters in the holographic lithography and $O_2$ plasma etching steps. By controlling the $O_2$ plasma etching parameters, periodic GNDs have also been obtained with the same processing method. Such large-area graphene nanopatterns with straightforward control of their dimensions and geometry could facilitate scale-up of GNM with potential applications in areas such as gas sensors,[9,17] light harvesters,[18,19] surface enhanced Raman sensors for rapid and nondestructive detection of molecules,[8] and nontoxic bio-imaging and related biomedical applications.[20]

## ACKNOWLEDGMENTS

This research was carried out in part at the Center for Functional Nanomaterials, Brookhaven National Laboratory, which is supported by the U.S. Department of Energy, Office of Basic Energy Sciences, under Contract No. DE-AC02-98CH10886. This research effort used resources in Micro Device Laboratory at Stevens Institute of Technology. The authors would like to thank Anthony Palumbo at Stevens Institute of Technology for helpful comments. This work was supported in part by the National Science Foundation (EECS-1040007, ECCS-1104870, and EEC-1138244), Air Force Office for Scientific Research (FA9550-12-1-0326), and the Office of Naval Research (N00014-11-1-0841).

[1]K. I. Bolotin, K. Sikes, Z. Jiang, M. Klima, G. Fudenberg, J. Hone, P. Kim, and H. Stormer, Solid State Commun. **146**, 351 (2008).
[2]A. K. Geim and K. S. Novoselov, Nat. Mater. **6**, 183 (2007).



Redistribution subject to AVS license or copyright; see http://scitation.aip.org/termsconditions. Download to IP: 74.102.104.224 On: Thu, 11 Sep 2014 13:24:11

[3]B. Huard, J. Sulpizio, N. Stander, K. Todd, B. Yang, and D. Goldhaber-Gordon, Phys. Rev. Lett. **98**, 236803 (2007).
[4]J. Lee, T.-J. Ha, H. Li, K. N. Parrish, M. Holt, A. Dodabalapur, R. S. Ruoff, and D. Akinwande, ACS Nano **7**, 7744 (2013).
[5]F. Schwierz, Nat. Nanotechnol. **5**, 487 (2010).
[6]F. Bonaccorso, Z. Sun, T. Hasan, and A. C. Ferrari, Nat. Photonics **4**, 611 (2010).
[7]T. H. Han, Y.-K. Huang, A. T. L. Tan, V. P. Dravid, and J. Huang, J. Am. Chem. Soc. **133**, 15264 (2011).
[8]J. Liu, *et al*., J. Phys. Chem. C **116**, 15741 (2012).
[9]R. K. Paul, S. Badhulika, N. M. Saucedo, and A. Mulchandani, Anal. Chem. **84**, 8171 (2012).
[10]Z. Cheng, Q. Li, Z. Li, Q. Zhou, and Y. Fang, Nano Lett. **10**, 1864 (2010).
[11]L. James and P. Balaji, Nanotechnology **23**, 265203 (2012).
[12]S. Bae *et al*., Nat. Nanotechnol. **5**, 574 (2010).
[13]K. S. Kim, *et al*., Nature **457**, 706 (2009).
[14]Z.-L. Wang, D. Xu, H.-G. Wang, Z. Wu, and X.-B. Zhang, ACS Nano **7**, 2422 (2013).
[15]X. Li, Y. Zhu, W. Cai, M. Borysiak, B. Han, D. Chen, R. D. Piner, L. Colombo, and R. S. Ruoff, Nano Lett. **9**, 4359 (2009).
[16]K. Kumar, Y.-S. Kim, X. Li, J. Ding, F. T. Fisher, and E.-H. Yang, Chem. Mater. **25**, 3874 (2013).
[17]A. Esfandiar, N. J. Kybert, E. N. Dattoli, G. Hee Han, M. B. Lerner, O. Akhavan, A. Irajizad, and A. T. Charlie Johnson, Appl. Phys. Lett. **103**, 183110 (2013).
[18]M. Begliarbekov, O. Sul, J. Santanello, N. Ai, X. Zhang, E.-H. Yang, and S. Strauf, Nano Lett. **11**, 1254 (2011).
[19]Q. Zhang, *et al*., Nano Res. **6**, 478 (2013).
[20]Z. Fan, Y. Li, X. Li, L. Fan, S. Zhou, D. Fang, and S. Yang, Carbon **70**, 149 (2014).
[21]M. Kim, N. S. Safron, E. Han, M. S. Arnold, and P. Gopalan, Nano Lett. **10**, 1125 (2010).
[22]X. Liang, Y.-S. Jung, S. Wu, A. Ismach, D. L. Olynick, S. Cabrini, and J. Bokor, Nano Lett. **10**, 2454 (2010).
[23]J. Bai, X. Zhong, S. Jiang, Y. Huang, and X. Duan, Nat. Nanotechnol. **5**, 190 (2010).
[24]A. Siitskii and J. M. Tour, J. Am. Chem. Soc. **132**, 14730 (2010).
[25]L. Liu, Y. Zhang, W. Wang, C. Gu, X. Bai, and E. Wang, Adv. Mater. **23**, 1246 (2011).
[26]Z. Zeng, *et al*., Adv. Mater. **24**, 4138 (2012).
[27]M. Wang, L. Fu, L. Gan, C. Zhang, M. Rümmeli, A. Bachmatiuk, K. Huang, Y. Fang, and Z. Liu, Sci. Rep. **3**, 1238 (2013).
[28]O. Akhavan, ACS Nano **4**, 4174 (2010).
[29]X. Ye and L. Qi, Nano Today **6**, 608 (2011).
[30]S. Park, J. M. Yun, U. N. Maiti, H.-S. Moon, H. M. Jin, and S. O. Kim, Nanotechnology **25**, 014008 (2014).
[31]X. Wang, J. He, J. Ma, J. Ding, J. Chu, and W. Huang, Opt. Eng. **50**, 054302 (2011).
[32]J. Ding, Z. Zhai, J. He, J. Li, X. Wang, and W. Huang, *5th IEEE International Conference on Nano/Micro Engineered and Molecular Systems (NEMS)* (2010), pp. 1074–1078.
[33]I. Wathuthanthri, W. Mao, and C.-H. Choi, Opt. Lett. **36**, 1593 (2011).
[34]W. Mao, I. Wathuthanthri, and C.-H. Choi, Opt. Lett. **36**, 3176 (2011).
[35]I. Wathuthanthri, Y. Liu, K. Du, W. Xu, and C.-H. Choi, Adv. Funct. Mater. **23**, 608 (2013).
[36]X. Zhang, M. Theuring, Q. Song, W. Mao, M. Begliarbekov, and S. Strauf, Nano Lett. **11**, 2715 (2011).
[37]X. Zhang and S. Strauf, Appl. Phys. Lett. **102**, 093110 (2013).
[38]K. Du, I. Wathuthanthri, W. Mao, W. Xu, and C.-H. Choi, Nanotechnology **22**, 285306 (2011).
[39]K. Du, I. Wathuthanthri, Y. Liu, Y. T. Kang, and C.-H. Choi, Nanotechnology **25**, 165301 (2014).
[40]K. Du, Y. Liu, I. Wathuthanthri, and C.-H. Choi, J. Vac. Sci. Technol., B **31**, 06FF04 (2013).
[41]K. Du, Y. Liu, I. Wathuthanthri, and C.-H. Choi, J. Vac. Sci. Technol., B **30**, 06FF04 (2012).
[42]K. Du, I. Wathuthanthri, Y. Liu, W. Xu, and C.-H. Choi, ACS Appl. Mater. Interfaces **4**, 5505 (2012).
[43]Y. Liu, K. Du, I. Wathuthanthri, and C.-H. Choi, J. Vac. Sci. Technol., B **30**, 06FF10 (2012).
[44]T. Lindeberg, Int. J. Comput. Vision **11**, 283 (1993).
[45]K. Kumar, Y.-S. Kim, and E.-H. Yang, Carbon **65**, 35 (2013).
[46]Z. Ni, Y. Wang, T. Yu, and Z. Shen, Nano Res. **1**, 273 (2008).
[47]L. Jiao, X. Wang, G. Diankov, H. Wang, and H. Dai, Nat. Nanotechnol. **5**, 321 (2010).
[48]N. S. Safron, M. Kim, P. Gopalan, and M. S. Arnold, Adv. Mater. **24**, 1041 (2012).
[49]J. Lee *et al*., Nano Lett. **12**, 6078 (2012).



Redistribution subject to AVS license or copyright; see http://scitation.aip.org/termsconditions. Download to IP: 74.102.104.224 On: Thu, 11 Sep 2014 13:24:11